8-2018

3D-Printed Fluidic Devices and Incorporated Graphite Electrodes for Electrochemical Immunoassay of Biomarker Proteins

Abdulhameed Alabdulwaheed
East Tennessee State University

Follow this and additional works at: https://dc.etsu.edu/etd

Part of the Analytical Chemistry Commons, Diagnosis Commons, and the Medical Biochemistry Commons

Recommended Citation

3D-Printed Fluidic Devices and Incorporated Graphite Electrodes for Electrochemical

Immunoassay of Biomarker Proteins

_____

A thesis

presented to

the faculty of the Department of Chemistry

East Tennessee State University

In partial fulfillment

of the requirements for the degree

Master of Science in Chemistry

_____

by

Abdulhameed Alabdulwaheed

August 2018

_____

Committee Chair, Dr. Greg Bishop

Committee Member, Dr. Dane W. Scott

Committee Member, Dr. Catherine McCusker

Keywords: 3D Printing, Electrochemistry, Immunoassay, Fluidics, Biomarkers

ABSTRACT

3D-Printed Fluidic Devices and Incorporated Graphite Electrodes for Electrochemical

Immunoassay of Biomarker Proteins

by

Abdulhameed Alabdulwaheed

Biomarkers are measurable indicators of health status or disease state that can be used for diagnosis and may help guide patient treatment strategies. Enzyme-linked immunosorbent assays (ELISA) and other many clinical techniques currently used for measuring biomarker proteins lack sensitivity, demand high analysis cost, are often not well-suited for measuring multiple biomarkers in a single sample, and require long analysis times. Here, we demonstrate simple, low-cost 3D-printed flow-through devices with integrated electrodes modified with gold nanoparticles (AuNPs) for electrochemical immunoassays of S100B, a biomarker protein related to conditions like skin cancer and brain injuries. Flow-through devices are fabricated from photocurable-resin using a desktop digital light processing (DLP) projector-based 3D printer to produce 500-800 μm square cross-sectional fluidic channels. Threaded ports at the ends and center of the channel are included in the device design for connecting commercially available fittings for fluid delivery and integrating low-cost graphite electrodes for electrochemical biosensing.

DEDICATION

I would like to dedicate this work and effort to my parents, brothers, sisters, and friends.

ACKNOWLEDGMENTS

TABLE OF CONTENTS

LIST OF FIGURES

LIST OF ABBREVIATIONS

BSA: Bovine serum albumin

Ab_1: Capture antibody

CAD: Computer-design

CV: Cyclic voltammetry

Ab_2: Detection antibody

DLP: Digital light processing

EDC: 1-ethyl-3-(3-dimethylaminopropyl) carbodiimide

FDM: Fused deposition modeling

GSH-AuNPs: Glutathione-capped gold nanoparticles

HRP: Horseradish peroxidase

LbL: Layer-by-layer

MBs: Magnetic beads

NHS: N-hydroxysuccinimide

NSB: Nonspecific binding

PBS: Phosphate buffered saline

POCT: Point-of-care testing

PDDA: Poly(diallydimethylammonium chloride)

SLS: Sodium lauryl sulfate

SLA: Stereolithography

CHAPTER 1

INTRODUCTION

Protein Biomarkers and Enzyme-Linked Immunosorbent Assays

Biomarkers are measurable indicators of a patient's health status that can be used for diagnostic purposes, such as determining disease state or evaluating response to treatment.[1] Since illnesses, infections, and malignancies activate and alter various responses of the immune system, biomarkers include biomolecules (e.g. proteins, nucleic acids, metabolites, etc.) present in biological tissues and body fluids.[2] For instance, C-reactive protein is a biomarker found in human serum that gives information about inflammation rates in colon cancer patients to help assess progression. Another example of a currently trending biomarker protein is transferrin, which is used to diagnose the rate of iron overload – a major cause of liver cancer.[3]

Clinical measurements of protein biomarkers are largely based on traditional enzyme-linked immunosorbent assay (ELISA).[4] ELISA is based on highly specific binding interactions between the antigen (protein analyte) and antibodies, which are used to isolate the analyte from the rest of the sample components and/or label the sequestered analyte with a signal-transducing enzyme. In traditional sandwich-type ELISA, the analyte is first collected from the sample using antibodies bound on a surface like that of a 96-well microplate (Figure 1). After washing to remove unbound sample components, a second antibody with an enzyme attached to it is introduced into the well with the captured antigen. Exposure of the enzyme to its substrate typically leads to the formation of a product that strongly absorbs visible light, thereby confirming the presence of analyte.[5,6]
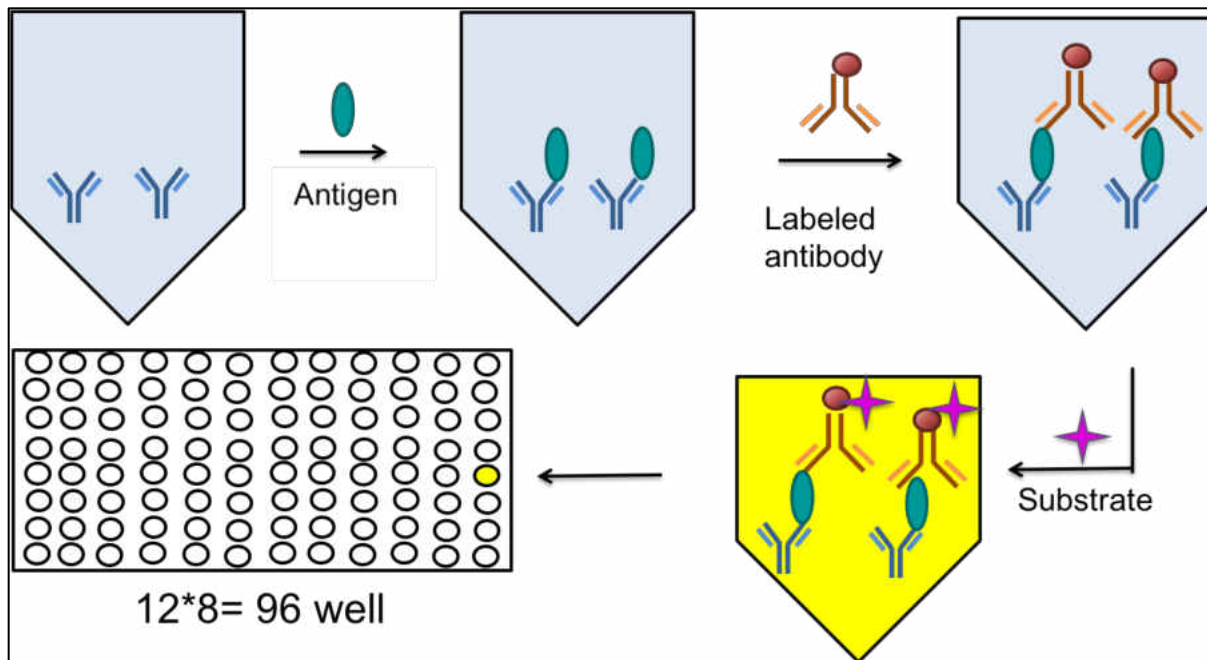
Figure 1: Illustrated schematic of a simple sandwich-type ELISA[5,7]

However, these methods often require relatively long analysis times, relatively large amounts of sample (~100 μL), substantial technical expertise, and a centralized lab environment.[6,7] Indeed, traditional ELISAs are not compatible with point-of-care-testing (POCT) and applications in resource-limited settings, which are two major areas of interest in bioanalytical research. This is due to high cost of the commercially available ELISA kits, advanced instrumentation requirements, and need for trained personnel.[8,9] Moreover, detection limits of standard ELISA techniques (typically 1-100 pg/mL) are often insufficient for detecting biomarker proteins during early stages of cancer or in some cases of cancer recurrence when biomarker levels are low.[4] Though studies have found that diagnostics based on multiple biomarker measurements can give better understanding of patient status than single biomarker measurements, ELISA is also generally not well-suited for measuring multiple biomarker proteins simultaneously, Consequently, there is considerable interest in developing novel, simple, fast, low-cost, and reliable detection strategies for measuring protein biomarkers.[10]

Electrochemical Biosensors

Due to the relatively low costs and lack of maintenance associated with electrochemical instrumentation, along with simplicity and relative ease of miniaturization, electrochemical biosensors have emerged as particularly viable technologies for developing new sensors for biomarker proteins.[11,12] Electrochemical biosensors convert a biological recognition event into a measurable electrochemical signal. Essentially, binding of a protein to a receptor (or an antibody) or interaction of an enzyme with a substrate is carried out at or near a suitable electrode surface in a way that causes a change in the potential impedance or produces current due to the onset of an oxidation or reduction reaction. [11,12]

Historically, Heineman and Halsall were the first to develop immunoassays based on electrochemical detection in the 1980s.[13] Various strategies for electrochemical immunosensors based on electrodes chemically modified with antibodies to capture protein antigen from samples have been reported. Captured antigen can be labeled with various types of electroactive particles or enzymes that can produce electroactive species for signal generation and protein quantitation.[12] Heineman's development of flow-through microfluidic electrochemical biosensors in the early 2000s represented a particularly noteworthy advance for improving sensor performance. Compared to ELISA conducted using traditional well plates, electrochemical biosensing in microfluidics enables compatibility with smaller sample volumes, minimizes amounts of expensive antibodies and enzymes necessary for the analysis, and offers greater opportunities for miniaturization and automation.[14,15]

The Rusling group has recently built on these pioneering concepts of Heineman to produce ultrasensitive, flow-through electrochemical biosensors for protein biomarkers of diseases like prostate cancer and oral cancer.[16,17] Rusling et al. have developed simple

polydimethylsiloxane (PDMS) fluidic devices interfaced with electrode arrays. PDMS channels (made using machined metal molds) are sandwiched between two hard plastic plates. Screen-printed carbon electrode arrays are positioned in the channel and modified with gold nanoparticles and antibodies. Antigen is collected from the sample in a microcentrifuge tube using magnetic beads modified with antibodies and an enzyme label. Magnetic beads are introduced into the fluidic device and those that have bound antigen are immobilized by the antibody on the electrode surface. Signal is generated by activation of the enzyme and use of a small diffusible redox species. Multiple proteins can be determined simultaneously with this system by modifying different electrodes in the same array with appropriate antibodies and preparing magnetic beads with similarly appropriate antibodies.[18]

In one study, using this system, Chikkaveeraiah el at. were able to detect interleukin-6 (IL-6) and prostate specific antigen (PSA) at low fg/mL levels in serum samples using flow-through amperometry as the detection method.[18] In another study, Malhotra et al. utilized the same fluidic device for simultaneous measurement of vascular endothelial growth factor C (VEGF-C), VEGF, IL-6, and IL-8 in human serum samples as a four-biomarker panel related to head and neck squamous cell carcinoma (HNSCC). This work showed good correlation to ELISA results for each cancer biomarker in a cohort of 78 patient samples, though the electrochemical biosensor required only 5 µL of sample and exhibited 100-1000 times lower detection limits than the traditional ELISA method.[19]

While the simple fluidic devices employed by Rusling et al. enabled high sensitivity and compatibility with low sample volumes, PDMS used for the channels is not well-suited for large-scale production or processing outside of research laboratory settings for point-of-care testing

(POCT).[20] As a result, 3D printing has been recently explored by Bishop et al. [21] and others[22,23,24,27,35,49] as an alternative method for preparing fluidic devices.

<u>3D Printing Technology and Fluidic Devices</u>

In 3D printing, a three-dimensional model of the desired object is first designed using computer-aided design (CAD) software. The design is processed to generate printer instructions which are sent to the 3D printer. Finally, the 3D printer builds the object by depositing or curing successive thin layers of material until the desired object is created. Printing material can be plastic, liquid, powder, or metal.[25]

Historically, Charles W. Hull was the first to invent 3D printing systems back in the early 1980s as he first fabricated plastic devices by curing successive layers of photopolymers through a technique called stereolithography (SLA).[26] Though 3D printers have been commercially available since 1988,[27] efforts to improve accessibility and affordability of 3D printers began in the mid-2000s through initiatives like the Rep-Rap project and Fab@Home program, which created communities aimed at developing and sharing ideas for improving 3D printers.[28,30] The successes of these programs generated interest in 3D printing technology and applications making 3D printers more affordable.

Several types of 3D printing technologies have been developed. These technologies vary from one another in the working mechanism and printing materials being used. Printing accuracy and price are essential features that must be considered. Of the available 3D printing technologies, printers based on stereolithography (SLA) and fused deposition modeling (FDM) systems are the most affordable, with desktop printers of these types ranging from a few hundred to a few thousand dollars. [20] In a recent study, Nordin et al. reported that SLA based on digital

light processing (DLP) generally exhibits better resolution than other methods for preparing fluidic devices.[31,33]

Principle of Stereolithography (SLA)

As previously mentioned, SLA depends on a photopolymerization mechanism. Resins are either acrylate or epoxy-based and contain a photoinitiator that causes the resin to harden when exposed to light.[32,33] A digital light-processing (DLP) projector, laser, or other light source is positioned underneath the resin reservoir. The light source transmits an image corresponding to a single layer of the design through a clear window at the bottom of the reservoir to cure photosensitive resin in a layer-by-layer fashion (Figure 2). The stage moves upward after each layer is created. Each successive layer is made in the same way until the 3D object is fabricated from bottom to top.[28] Exposing the resin with a DLP projector in a layer configuration has been reported to be faster in fabricating the object compared to laser-based curing due to the capability of DLP to cure each successive layer of the object with single exposure steps.
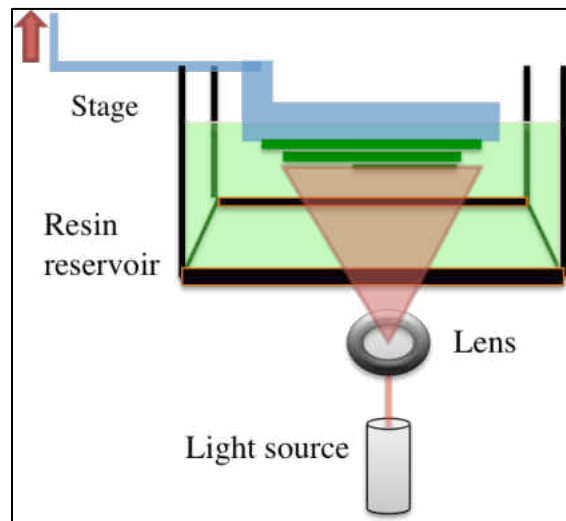
Figure 2: Illustrated schematic of a DLP projector-based 3D-printer[28]

Recent Developments in 3D-Printed Fluidic Devices

Fused deposition modeling (FDM) and Stereolithography (SLA), and other more expensive 3D printing methods have recently been employed to directly print fluidic devices. Compared to other methods of preparing fluidic devices like photolithography, 3D printing methods hold some advantages in that they do not require multiple processing steps or unique molds and masks for different fluidic designs, access to clean-room facilities, or large initial capital investments in expensive equipment.[32] Reproducible and reliable fabrication of fluidic devices with truly microfluidic dimensions is often complicated by factors such as overcuring of photopolymer resin and necessary removal of support materials included during printing processes.[32] Recently, 3D-printed fluidic channels with dimensions as small as 18 μm x 20 μm have been fabricated by Nordin et al.[29] using a DLP-SLA 3D printer and custom-formulated resin, However, research continues to lead to improvements in printer capabilities and materials for producing smaller fluidic devices, and millifluidic devices with channel dimensions of hundreds of micrometers can be prepared with reasonable success for various applications.

Sensors Based on 3D Printed Fluidics

Several biosensors based on 3D-printed fluidic devices paired optical detection methods, even some using smartphone cameras to measure optical signals,[24] have been described. The combination of 3D-printed fluidics with electrochemical detection methods has also been gaining considerable interest for developing biosensors. The pairing of 3D printing with electrochemical instrumentation can provide relatively inexpensive, robust and easy to operate platforms for biosensing compatible with several important areas of need such as POCT applications and low-cost devices for resource-limited settings.[20]

In 2010, Snowden et al. demonstrated one of the first approaches toward developing 3D-microfluidic devices for versatile electrochemical measurements. They utilized a 3D-printing service to produce flow-cell designs based on an expensive microstereolithography (MSL) printer and resin consisting of a proprietary mixture of polymers.[34] Flow-cells consisted of devices that featured 3-sided open-bottom channels with widths of 3 mm and heights of 200 μm, which were placed on top of electrodes deposited on a planar surface like an Si/SiO2 wafer. Devices featured inlet and outlet ports and a leak-proof seal was created between the electrode substrate and the bottom of the channel simply by fastening the device and electrode substrate together using cotton thread. Microfluidic device functionality for electrochemical measurements was confirmed through the series of experiments using redox probes at various flow rates.

Erkal et al. developed 3D-printed devices with incorporated electrodes for electrochemical measurement of nitric oxide (NO), oxygen tension in a stream of red blood cells, and the neurotransmitter dopamine. Fluidic devices with channel sizes of 500 x 500 μm were printed using an expensive Objet Connex 350 polyjet 3D printer. Electrodes were introduced into the device through threaded ports that are compatible with commercially available fittings into which metal wires can be inserted to serve as electrodes.[22]

Bishop et al. demonstrated that electrodes could similarly be incorporated in semitransparent 3D-printed microfluidic devices produced using a very low cost FDM printer.[21] The fluidic device was fabricated using transparent polyethylene terephthalate (PET) filament and featured threaded ports to access the fluidic channel. Custom-threaded fittings for electrode integration into the device channels were fabricated using thermoplastic polymer, acrylonitrile butadiene styrene (ABS) since printer resolution was not sufficient to facilitate use of commercially available fittings. Gold disk working electrodes were made of Au wire integrated

16

in the ABS fitting. Prussian blue nanoparticles (PBNPs) were prepared using a separate 3D-printed flow mixing device and deposited on Au electrodes for sensing of hydrogen peroxide (H_2O_2). The 3D-printed flow devices with integrated PBNP-modified Au electrodes exhibited excellent response towards different concentrations of H_2O_2 using a flow-through amperometric method. In a separate report, Bishop et al. developed transparent fluidic devices via a desktop DLP-SLA printer that could be interfaced with low-cost graphite electrodes through commercial fittings and compatible printed threaded ports for electrochemiluminescence measurements of DNA oxidation.[23]

Research Objectives

ELISAand other clinical techniques for measuring biomarkers proteins typically lack sensitivity, demand high analysis cost, are often not well-suited for measuring multiple biomarkers in a single sample, and require long analysis times. Hence, the primary goal of the work described herein is to develop a simple, low-cost 3D-printed flow-through device with modularly integrated electrodes to serve as a platform for electrochemical sandwich-type immunoassays. For the biomarker protein target for immunoassay development in these studies, we selected the protein S100B, which is a biomarker for melanoma, one of the most prevalent forms of cancer in the United States ranking as the 5th most common cancer among men and 6th most common among women.[36] Over the past few decades, the number of new cases of melanoma has consistently increased, and it is expected to continue to grow at a rate that is among the highest of all cancers.[37,38] Even though melanoma accounts for less than 5% of all forms of skin cancers,[39] it is responsible for the vast majority of deaths caused by the disease.[36]

High levels of S100B in tissues and serum are commonly related to stage III and IV disease and are used in national guidelines in other countries for diagnosis of melanoma.[40,41,42] One study of 412 healthy individuals and 1,007 melanoma patients found the geometric mean in sera of healthy controls to be 20 pg/mL.[42] On the other hand, 12% of melanoma patients in clinical stage I, 51% in stage II, and 79% in stage III had levels greater than 100 pg mL^{-1}. In another study, von Schoultz et al. analyzed 643 patient samples with varying clinical stages of malignant melanoma. It was found that the relative risk of death increased five-fold when the average of S100B surpassed 0.6 ng/mL.[43]

In working towards accomplishing the objective of demonstrating an immunosensor platform and strategy for S100B based on 3D-printed fluidics and electrochemical detection, we combined elements from the electrochemical 3D-printed fluidic devices described by Bishop et al. with the detection strategy outlined by the Rusling group. In this project, a DLP projector-based 3D printer was utilized to fabricate fluidic devices from photoactive resin with slightly smaller limiting channel dimensions compared to those previously reported using a laser-based SLA printer. Electrodes were made from low-cost pencil graphite and commercially available threaded fittings. The sandwich-type electrochemical immunoassay was adapted from previous reports from the Rusling group.[18,19,46]

CHAPTER 2

EXPERIMENTAL

Chemicals and Materials

Sodium chloride, sodium phosphate dibasic, and potassium phosphate monobasic were purchased from Acros Organics. Sulfuric acid (95-98%), potassium chloride, hydroquinone (≥99%), hydrogen peroxide (30% wt in H_2O), poly(diallyldimethylammonium chloride) (PDDA) (20 wt% in water, M_w 350,000 to 400,000), Tween-20, and 2,2'-azino-bis(3-rthylbenzothiazoline-6-sulphonic acid) (ABTS) were obtained from Sigma Aldrich. Potassium ferricyanide, citric acid, and sodium lauryl sulfate (SLS) were from Fisher Scientific. Diagnostic grade probumin Bovine Serum Albumin (BSA) was obtained from Millipore. Hydrochloric acid (36.5-38%) and sodium hydroxide were acquired from VWR. Magnetic microbeads (ProMag 1) were procured from Bangs Laboratories, Inc. N-Hydroxysuccinimide (NHS) (98+%) and 1-Ethyl-3-(3-dimethylaminopropyl) carbodiimide (EDC) were obtained from Alfa Aesar. Biotinylated peroxide, horseradish peroxidase enzyme (HRP) was supplied by Invitrogen. Human S100B protein, S100B capture antibody, and S100B detection antibody were acquired from R&D Systems Company. Photopolymer PR48-clear resin was procured from Autodesk. Photopolymer B9R-4-Yellow resin was purchased from B9Creations. All solutions were prepared using 18.2 MΩ ultrapure water, which was obtained by passing deionized water through a Millipore Synergy UV water purification system.

Fabrication of 3D-Printed Fluidic Devices

A B9Creator v1.2 DLP projector-based SLA 3D-printer (B9 creations) (Figure 3) with XY resolution reaches to 30 μm was used to prepare flow-cell devices, which were designed using 123D Design computer-aided design (CAD) software (Autodesk). The fluidic device

design was generally based on previous work of Bishop et al.[21,23] Threaded ports located at the inlet and outlet of the channel provided means for fluid delivery using commercially available fittings and tubing, and a threaded port in the center of the device enabled incorporation of electrodes. The design file was processed using B9Creator software to configure printing parameters and generate SLA instructions by slicing the 3D representation into sections of user-defined thickness along the z-axis. The resulting SLA file was uploaded to the 3D printer, and the object was printed.
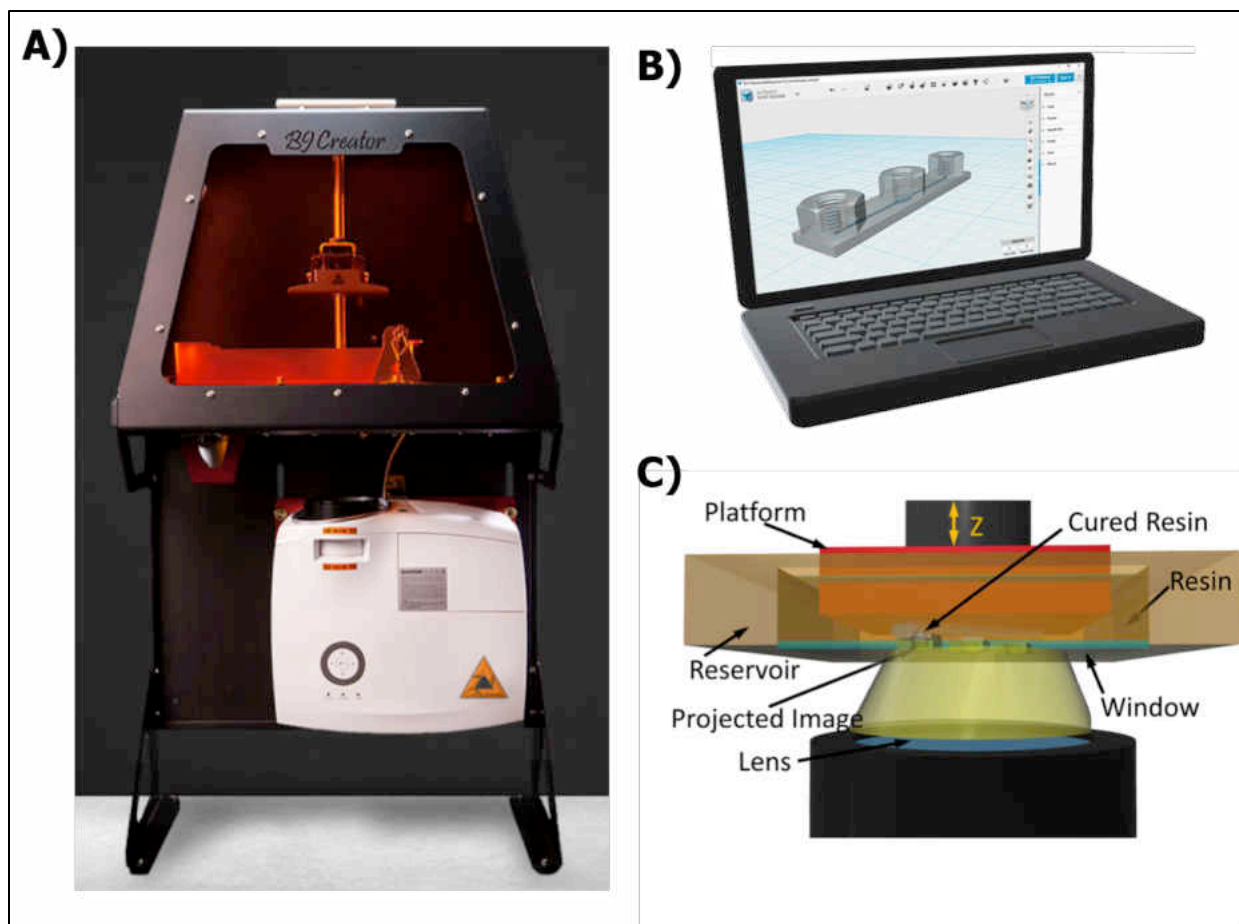
Figure 3: Photograph of B9Creator 3D-printer and illustrated representation of the printing process. A) Photograph of 1.2v B9Creator with DLP-based projector. B) A digital representation of the desired object is prepared using computer-aided design (CAD) software. C) Illustrated representation of the printing process based on SLA printing with DLP-based projector

Electrode Fabrication

Electrodes were incorporated into commercially available fittings as has been previously

reported by Erkal et al.[22] and Bishop et al.[21,23], so that they could be integrated into the 3D-

printed fluidic device. Electrodes were prepared from various conductive wires or rods (0.25 or

0.50 mm in diameter) that were connected to 24-gauge copper wire (Figure 4). These wires were

inserted into the center hole of commercially available 10-24 threaded fittings such that the

conductive wires or rods were located at the bottom of the fitting opening. Empty space between

the wires and center hole of the fitting was filled with epoxy, and the fitting was polished,

resulting in disk shaped-electrodes.
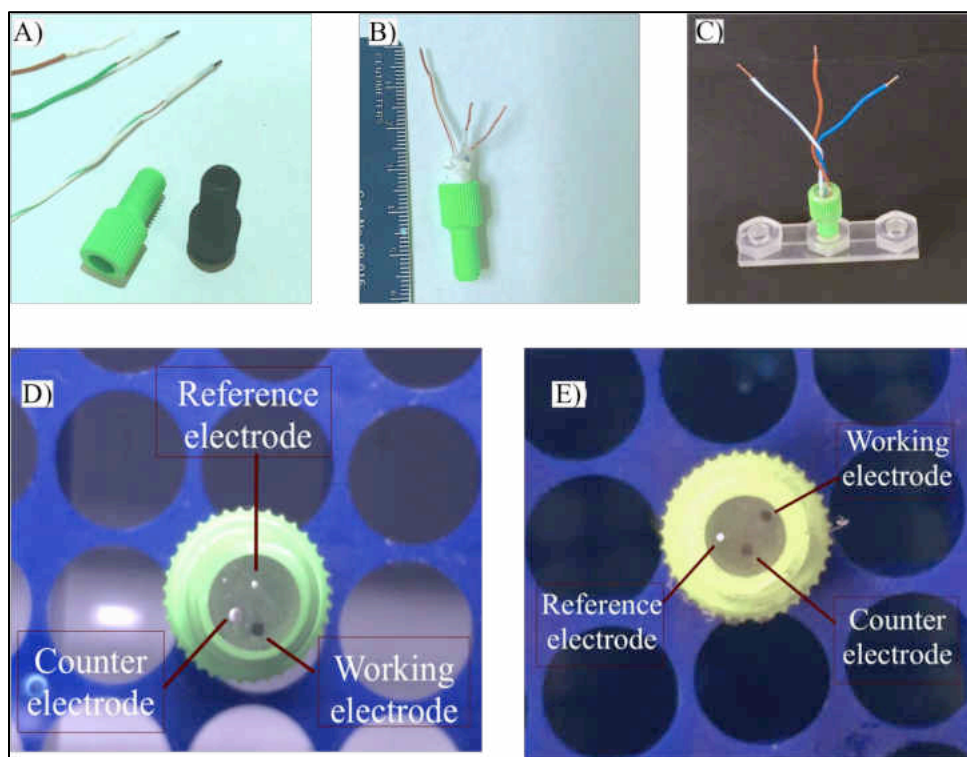
Figure 4: Photographs of electrodes fabricated in commercially available fittings. Images of electrode components (A) and assembled electrodes (B). C) Side view of assembled electrode incorporated into transparent 3D-printed device with straight design. (D) Bottom view of graphite working and counter electrode (stainless steel counter electrode in D)

Each electrode fitting contained at least 3 electrodes, with at least one serving as the working electrode, one as the reference electrode, and one as the counter electrode. Electrode fittings featured carbon working electrodes that were fabricated using very low-cost pencil graphite rods (0.5 mm in diameter). Silver wire (0.25 mm in diameter) and 22-gauge stainless steel (SS) wire (0.64 mm in diameter) were used as the reference and counter electrodes, respectively.[21,22,23] For carbon and stainless-steel wire, one end of the wire was connected to 24-gauge Cu wire using Ag paste to provide a low resistance of (0-0.9 Ω) prior to insertion in the fitting. Since conductivity could be impaired by negligent manipulation of the wires, a digital multimeter was used to verify suitable resistance before and after the wires were inserted into the threaded fitting. For silver wire, one end of the wire was connected to 24-gauge Cu wire by soldering to give resistance of 0 Ω. The copper wires provide a means for connecting the electrodes to electrochemical workstations for measurements.

<center>Electrochemical Measurements</center>

After electrode fittings were fabricated and polished, silver disk electrodes coated with silver chloride were used to provide a suitable quasi-reference electrode for the system. This was achieved by connecting the silver disk electrode in the electrode fitting, which was placed in a 1.0 M HCl solution, to the anode of a 9-volt battery. The circuit was completed using a Pt wire or other silver chloride-coated silver wire also placed in the HCl solution. All electrochemical measurements were obtained using a CHI400 electrochemical analyzer or CHI1030C 8-channel multi-potentiostat. Cyclic voltammetry and amperometry were used to evaluate electrode fitting performance and complete electrochemical immunoassays.

Electrochemical Immunoassay

The electrochemical immunoassay strategy for S100B biomarker protein was adapted from previous work.[18,19,46] The strategy generally involves nanostructuring carbon working electrodes using electrostatic adsorption of glutathione-capped gold nanoparticles (GSH-AuNPs) and attaching capture antibodies to the free carboxylate ends of GSH-AuNPs through amide bond formation using EDC/NHS. The antibody-modified electrodes were integrated into the 3D-printed flow-cell. S100B proteins were collected from the sample using magnetic beads that were modified with antibodies and a signal-transducing enzyme label horseradish peroxidase (HRP). The collected proteins labeled with magnetic beads were introduced into the flow-cell through a flow injection system, where they were subsequently captured by the antibodies on the electrode surface. Signal was generated by activating the HRP enzyme using H_2O_2. The activated enzyme oxidized a small, diffusible molecule (hydroquinone), which then was reduced at the electrode upon application of a suitable potential using an electrochemical workstation.

Nanostructuring and Modification of Electrodes with Antibodies

GSH-AuNPs (~5 nm) were prepared according to the method of Zheng et al.[44] Following previous reports by Rusling et al.,[45] working electrodes were modified with GSH-AuNPs by a simple layer-by-layer (LbL) electrostatic adsorption method (Figure 5).[18,19] First, PDDA (2 mg/mL in 0.05 M NaCl) was deposited on carbon working electrodes by drop casting 2 µL of the PDDA solution on the electrode surface.
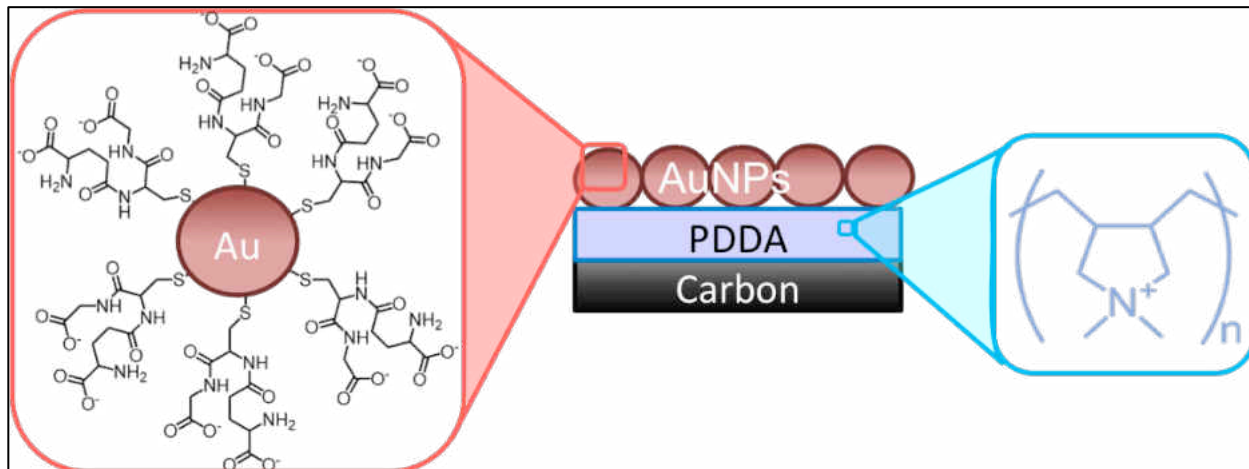
Figure 5: Illustrated representation of an electrode modified with gold nanoparticles using layer-by-layer (LbL) electrostatic adsorption

After rinsing with water and drying with nitrogen, GSH-AuNPs were similarly deposited by drop casting. After rinsing with water and drying, a mixture of EDC and NHS (375 mM/750 mM) was dropped on the electrode and allowed to sit on the electrode surface for 10 minutes to activate carboxylate groups. After activated electrodes were rinsed and dried, S100B capture antibodies with concentration of 240 µg/mL were then deposited on the electrode to immobilize them through amide bond formation.

Preparation of Antibody- and Enzyme-Labeled Magnetic Beads

Magnetic beads (MBs) functionalized with detection antibodies and HRP enzyme labels were prepared from streptavidin-coated MBs (~1 µm dia.) using a procedure that was adapted from previous literature,[18,19,46] and recommendations of the magnetic bead manufacturer.[53] Briefly, 20 µL of magnetic microbeads (0.2 mg) were washed three times with 200 µL volume of 0.1 M, Phosphate Buffered Saline (PBS. pH 7.3). A magnetic bead separator that consisted of a 3D-printed microcentrifuge tube holder and neodymium magnet (K & J magnetics) (Figure 6) was used to remove buffer after each wash, and the magnetic beads were resuspended after addition of new buffer solution by vortexing. After the final wash, the pellet was resuspended in

400 µL wash buffer to give a suspension with bead concentration of 0.5 mg/mL. The washed

MBs were split into four portions of 100 µL (0.05 mg each) in separate microcentrifuge tubes.
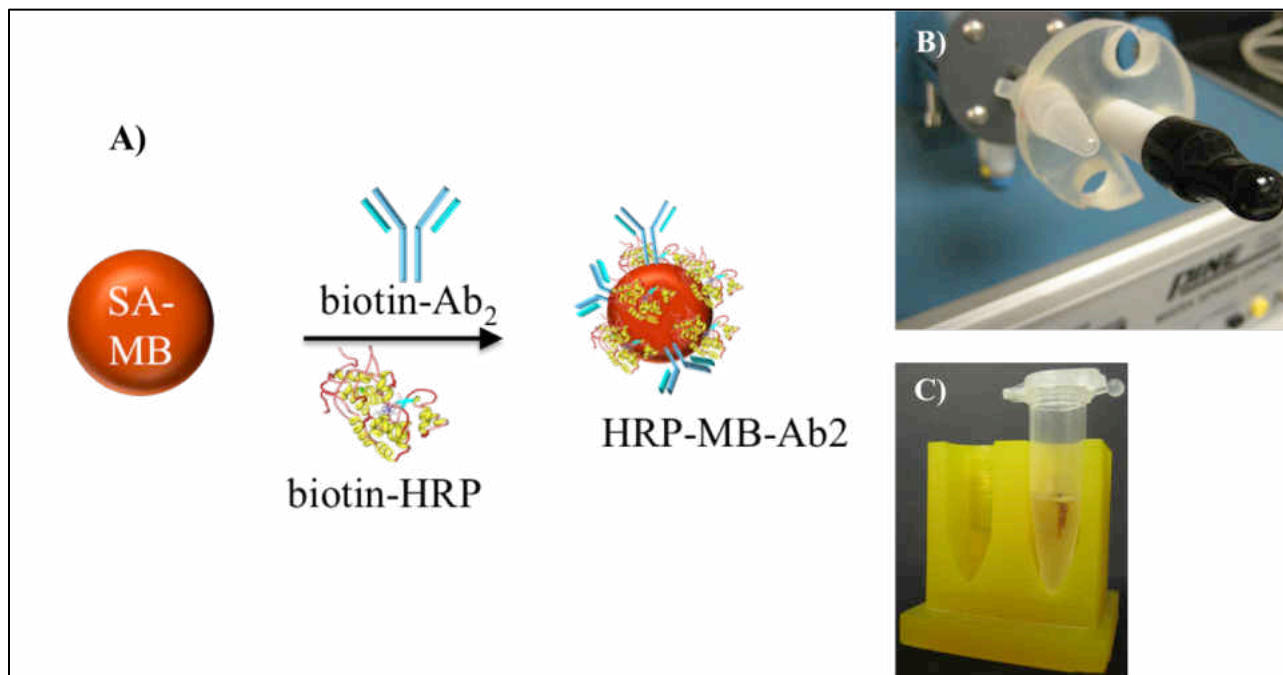
Figure 6: Illustration representation and photographs of the process of preparing the bioconjugate magnetic beads MBs

Biotinylated IgG detection antibody (Ab_2) for S100B (5 and 20 µL of 6 µg/mL) were

mixed separately with 15 µL of 0.25 mg/mL biotin-HRP prepared by diluting commercial biotin-

HRP reagent ten times with 0.1M PBS. The antibody-HRP mixtures were each diluted with

0.1M PBS to give a final volume of 35 µL, and added to separate 100 µL portions of magnetic

beads. The mixtures were quickly vortexed, and put on a microcentrifuge tube rotator, which

consisted of a 3D-printed microcentrifuge tube holder attached to an electrode rotator (Figure

6B) for 45 minutes. The mixture was washed 3 times with 100 µL 0.1M PBS and beads were

separated from solution after each wash. The magnetic bead conjugates were resuspended at a

final concentration of 0.5 mg/mL in 0.1M PBS.

Characterization of Bioconjugate MBs

To determine enzyme loading on bioconjugate MBs, an ABTS assay was performed.[54] HRP standards were prepared by diluting biotin-HRP in 0.1M PBS. MB bioconjugate samples were diluted 160x in 0.1M PBS. 40 µL of each standard and sample were placed in separate microcentrifuge tubes and kept cold in the fridge or on ice. ABTS, 600 µL of 1 mg/mL in phosphate citrate buffer (pH 5.0) with 0.03% hydrogen peroxide was added to each microcentrifuge tube and incubated at room temperature for 30 minutes. The reaction was stopped by adding 600 µL of 0.6% SLS. A blank was prepared by mixing 600 µL of phosphate-citrate and 600 µL of 0.6% SLS. Absorbance was measured at 420 nm for each reaction mixture using Shimadzu UV-VIS instrument.

Isolation and Labeling of Protein Biomarker

The electrochemical immunoassay for S100B was completed by first isolating the protein from the sample and labeling it with bioconjugate MBs. Magnetic beads bioconjugate, 30 µL of 0.5 mg/mL, prepared previously were mixed with 10 µL S100B biomarker protein sample or control (ultrapure water). The resulting mixture was put on the microcentrifuge rotator for 20 minutes at 400 RPM. After mixing, beads were then washed three times with 0.1M PBS, resuspended in 60 µL 0.1M PBS, and kept in fridge or ice until other processes have been completed.

Flow-Injection System

While MBs were incubated with S100B sample or control, an antibody-modified electrode was incorporated into the 3D-printed fluidic device. First, the electrodes in the fitting were rinsed with 0.1 % bovine serum albumin (BSA) in 0.1M PBS to help block non-specific binding of MBs on the electrode surface.[45] For better sealing of the commercial fitting threads

with the 3D-printed device threads, white Teflon tape was wrapped around the fitting, and then electrode fittings were secured into the center port of the 3D-printed flow-cell device. Inlet and outlet ports of the device were connected to fittings into which commercially available tubing had been inserted. The inlet tubing was also connected to a manual injector (Rheodyne, LLC) fitted with a 20 µL sample loop, which was in-line with a syringe pump (New Era Systems) to serve as a flow-injection system. The flow-injection system facilitated delivery of electrolyte solutions and reagents through the channel to the incorporated electrode. The flow rate was typically set to 100 µL/min.

Capture of Magnetic Bead-Labeled Protein Biomarkers and Development of Electrochemical Signal

BSA, 80 µL of 0.1 %, was loaded into sample loop, and injected under a flow of 0.05% Tween-20 surfactant in 0.1M PBS in order to passivate the surface of the flow-cell and electrode and reduce potential NSB. Flow was stopped for 5 minutes when BSA reached electrodes (20 seconds after injection), and flow was then resumed until the BSA was satisfactorily purged from the sample loop. MBs exposed to S100B sample or control were then introduced into the 3D-printed fluidic device under a flow of 0.1M PBS at rate of 100 µL/min. Again, flow was stopped, and MBs incubated on the electrode surface for 15 minutes to facilitate binding. Flow was resumed after the incubation step was complete to remove unbound MBs. Signal was generated by injecting a mixture of 100 µM hydrogen peroxide and 1.0 mM hydroquinone into the sample loop under a flow of 100 µL/min of 1.0 mM hydoquinone in order to activate the enzyme labels on the MBs and oxidize hydroquinone. Electrochemical reduction of oxidized hydroquinone provided a signal that was related to S100B concentration in sample being detected.

CHAPTER 3

RESULTS AND DISCUSSION

3D-Printed Fluidic Devices

With typical resolution of tens of micrometers in the XY dimensions and a few

micrometers to tens of micrometers in the Z dimension, SLA is among the best 3D-printing

methods for accurately producing objects with small dimensions. Two basic 3D-printed fluidic

device designs were used in these studies (Figure 7). A straight channel design featured inlet and

outlet ports that were in line with the central electrode port as previously reported by Bishop et

al.[21,23] except the overall channel and device length were shorter. The straight channel was

designed to have 800 μm x 800 μm square cross-sectional channel, 4.2 cm in length, with total

internal volume ~26 μL. A U-shaped channel design with the inlet and outlet ports offset from

the central port was also tested. The U-shaped channel was designed to be 500 μm wide by 600

μm high, 3.2 cm in length, and with total internal volume ~9.6 μL. While there were no

significant differences in overall device behavior, the U-shape design provides somewhat easier

incorporation of the electrode in the device due to the extra space given by the offset between the

inlet/outlet ports and the central electrode port.
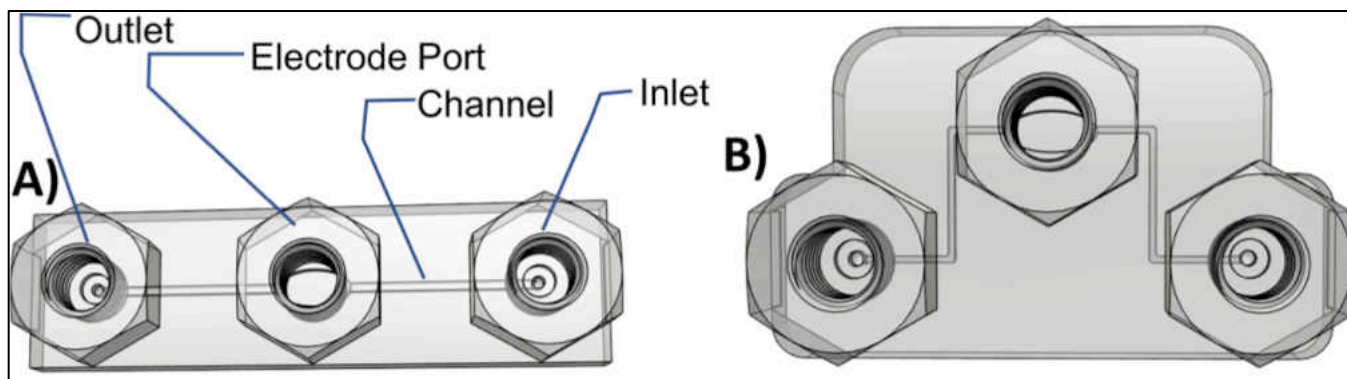
Figure 7: Illustrated representations of 3D-printed fluidic devices. A) Straight channel device.
B) U-shaped channel device

Fluidic devices of both types were fabricated from two different photocurable resins, PR48-clear resin and B9R-4-Yellow resin (Figure 8). All devices were printed at 50 μm XY and 50 μm Z resolution. The combination of channel design size and printing resolution enabled production of devices with open channels. However, printing occasionally led to partially or completely blocked channels, and in some cases, devices that were unusable. This is a common problem with fluidic devices produced by SLA and other printing methods where materials are initially present in the channel as it is developed.
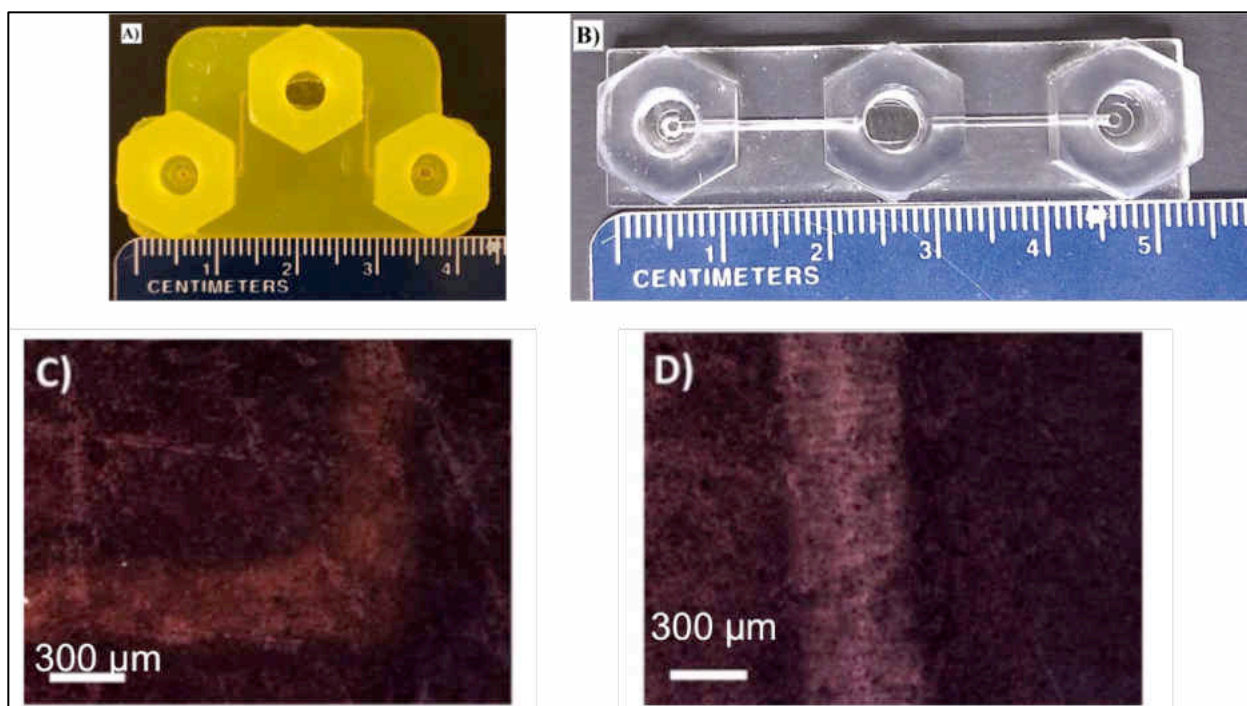
Figure 8: Photographs and microscope images of printed devices and channels. A and B are images of 3D-printed fluidic. C and D are microscope images of channels in 3D-printed fluidic devices. Scale bars represent 300 μm

Cross-sectional images of open-ended channels showed good agreement between channel design size and actual printed size (Figure 9). A straight channel designed to be 800 μm x 800 μm with total internal volume ~26 μL was found to measure 720 μm in height and 830 μm in width. The reduced height of the printed device compared to the design is most likely caused by

overcuring of the 50 μm z-axis sections due to bleeding of photoradiation in the z-axis during exposure steps.
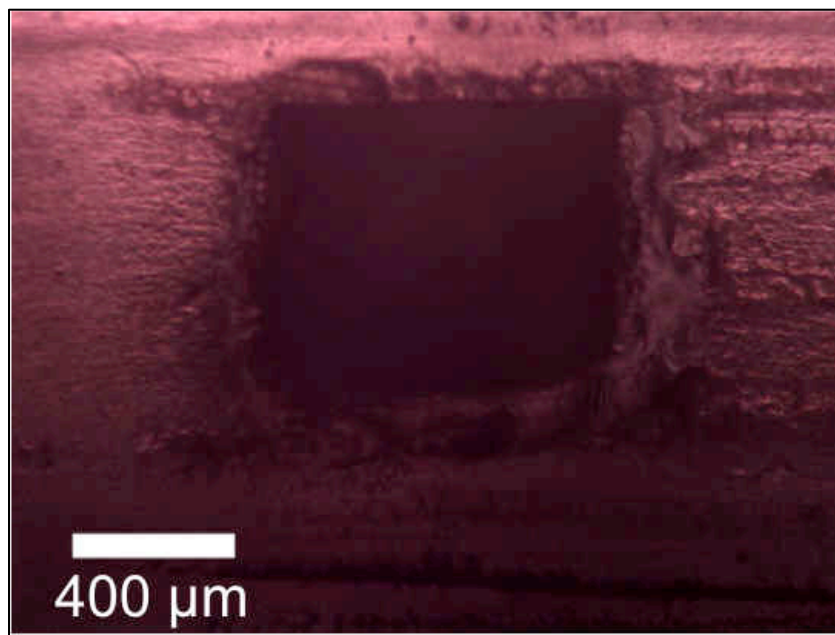
Figure 9: Microscopic images of cross-sectional view of straight channel

<u>Electrochemical Characterization of Electrode Fittings</u>

After fabrication of electrode fittings, the electrochemical behavior of the electrode system was tested through cyclic voltammetry (CV) of $K_3[Fe(CN)_6]$ as the redox probe at different scan rates to confirm functionality (Figure 10). Electrodes exhibited a typical peak-shaped response for ferri-/ferrocyanide redox couple showing a pair of peaks centered at 170.5 mV vs. Ag/AgCl and a peak separation of 79 mV. The CV peak current also showed a linear relationship with the square root of the scan rate as expected, which allowed application of the Randles-Sevcik equation to estimate the electroactive surface area of the pencil graphite working electrodes.

$$i_p = (2.686 \times 10^5)n^{3/2}AcD^{1/2}v^{1/2} \tag{1}$$

Where, i_p corresponds to peak current (in A), n is the number of electron transferred per mole of

redox active species during the electrochemical reaction, A is the electrode area (in cm^2), c is the

bulk concentration of the redox active species (in mol/cm^3), D is the diffusion coefficient (in

cm^2/sec), and v is the scan rate (in V/s).
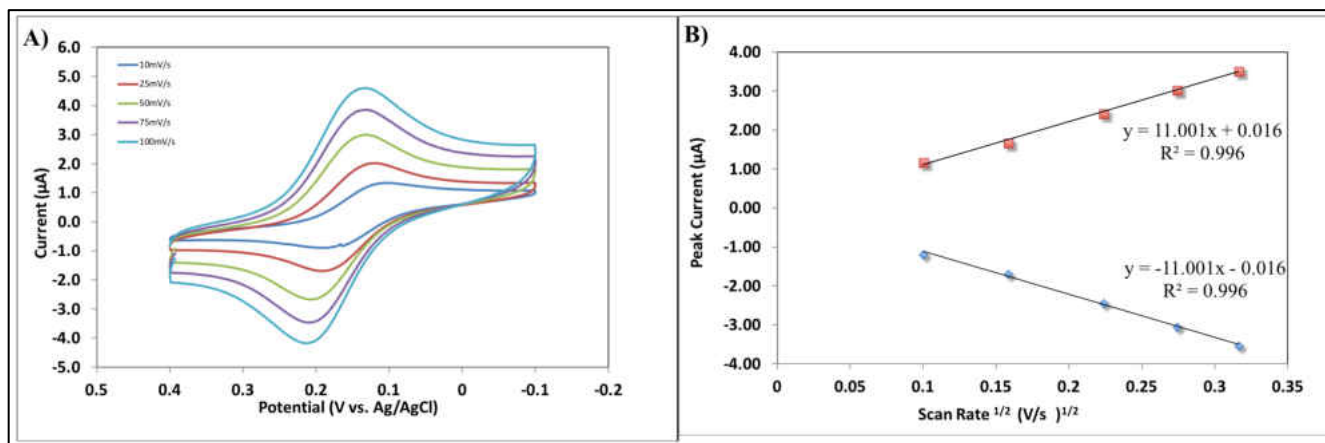
Figure 10: Electrochemical behavior of the electrode system. A) Representative CVs of electrode fitting in 1.0 mM $K_3[Fe(CN)_6]$ in 0.1 M KCl prepared in ultrapure water at different scan rates ranging from 10 mV/s to 100 mV/s. B) Randles-Sevcik plot for cathodic and anodic peak currents obtained from CVs

The average electroactive surface area estimated using equation 1 was 3.1 ($\pm$0.74) $x10^{-3}$

cm^2 (n = 6) with a 23.7% relative standard deviation (RSD). The nominal diameter for the pencil

graphite rod used in the fabrication of each working electrode was 0.5 mm. Hence, the geometric

area of the electrode is expected to be 2 x 10^{-3} cm^2. The discrepancy between the electroactive

surface area and the estimated geometric surface area may be indicative of surface roughness or

variations in orientation of the graphite rod in the fitting, which can result in different cross-

sectional electrode shapes (oval or circle). Variations in cross-sectional shape and surface

roughness can also contribute to differences in electroactive surface areas among electrodes

fabricated through the same procedure.

CVs were also obtained to ascertain electrochemical behavior of the electrode fittings in

the 3D-printed flow cell. Electrode fittings were first placed in a 10-mL beaker of the

K_3[Fe(CN)_6] solution so that CV measurements could be performed. The same electrode fittings were then incorporated into 3D-printed fluidic devices filled with the $K_3[Fe(CN)_6]$ solution using 10-mL syringe; thus, CV measurements could be repeated for comparison of responses inside and outside the channel.

There were no significant differences in peak positions or peak currents for electrodes in the beaker compared to electrodes in the 3D-printed fluidic devices (Figure 11). These results confirm the flow-cell system with incorporated low-cost electrodes can be used for reliable electrochemical measurements.
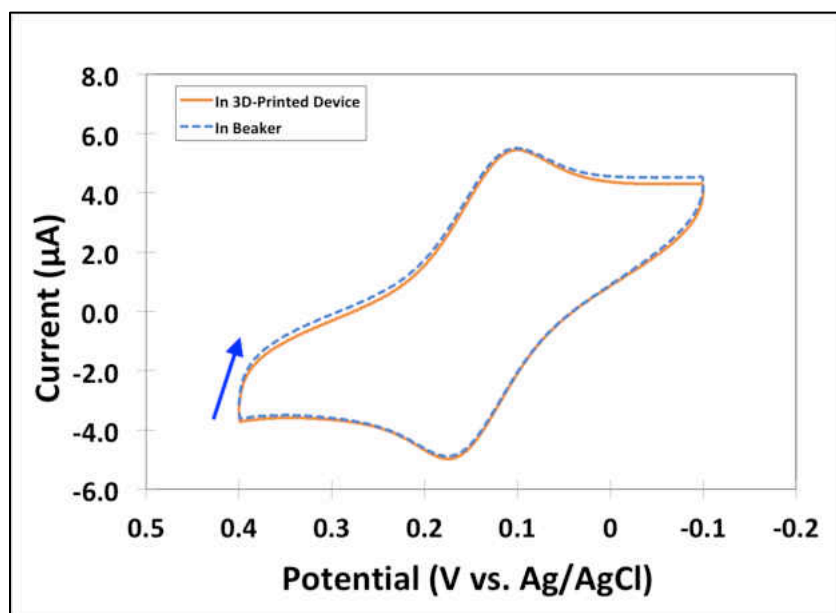
Figure 11: Comparison of CVs responses of electrode fitting towards the $[Fe(CN)_6]^{3-}$ /$[Fe(CN)_6]^{4-}$ redox couple for graphite electrodes inside and outside the 3D-printed fluidic device. CVs were obtained in 1.0 mM potassium ferricyanide with 0.10 M KCl prepared in ultrapure water at scan rates of 100 mV s^{-1}. Arrows indicate the direction of scans

Flow-Through Amperometry with Electrode in 3D-Printed Device

3D-printed fluidic devices with incorporated electrodes were connected to a syringe pump and manual injector to test compatibility with flow-through amperometry as an electrochemical detection method (Figure 12). The electrochemical response was tested by

injecting 20 µL of a mixture of 1.0 mM $K_3[Fe(CN)_6]$ (redox probe) and 0.10 M KCl electrolyte

prepared in ultrapure water under a 100 µL/min flow of 0.10 M KCl while the electrode was held

at a potential of 0 V vs. Ag/AgCl. A peak-shaped response was generated as the redox probe is

reduced once it reaches then flows past the working electrode. After injection, 20 seconds was

required for the current to reach a value that was 10% greater than the background, and another

9-10 seconds for the current to reach a maximum of 0.28-0.30 µA.
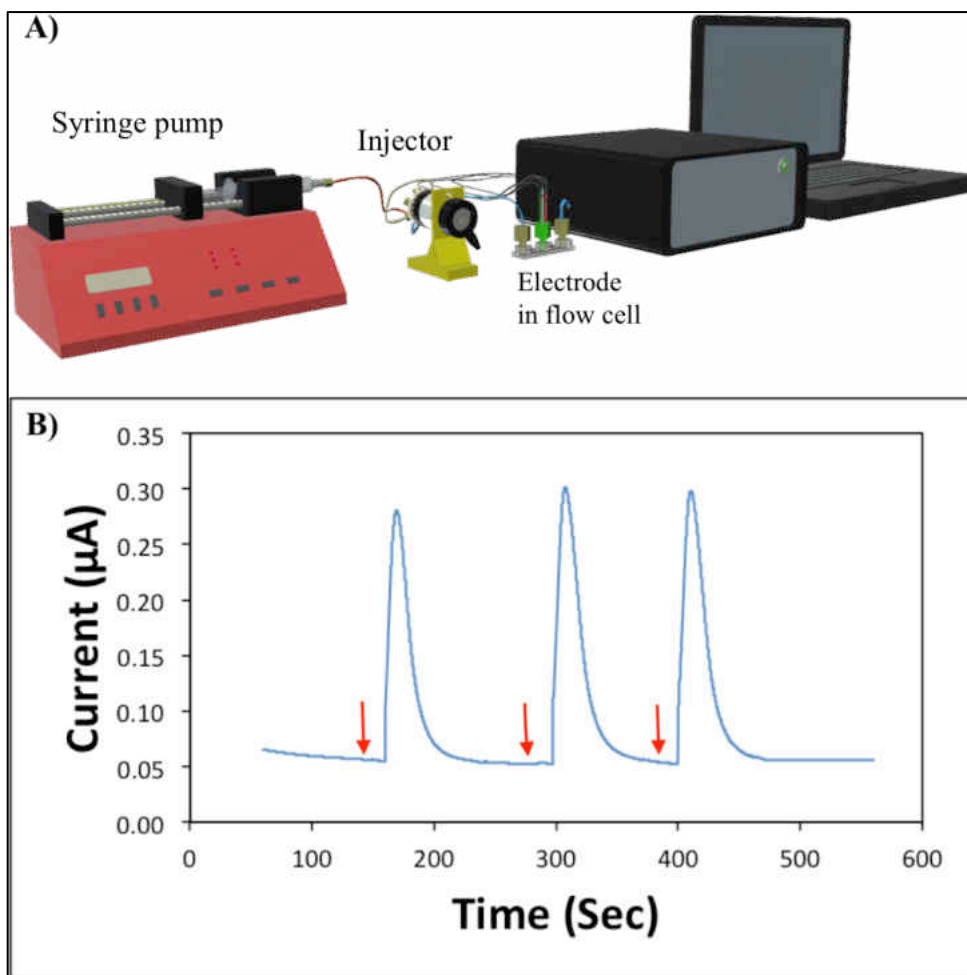
Figure 12: Flow-through amperometry setup and representative responses. A) Illustrated representation of the flow-through amperometry setup. The 3D-printed device with incorporated electrode is located downstream from a manual injector and syringe pump. B) Representative responses for 1 mM ferricyanide in 0.1 M KCl prepared in ultrapure water loaded and injected through a 20 µL sample loop at 150 sec, 280 sec, and 380 sec under a 100 µL/min flow of 0.1 M KCl while the working electrode was held at a potential of 0 V vs. Ag/AgCl

<u>Characterization of AuNP-Functionalized Pencil Graphite Working Electrodes and Modification</u>

<u>with Capture Antibodies</u>

Pencil graphite working electrodes were modified with antibodies to serve as platforms for the sandwich-type electrochemical immunoassay. Electrode modification was accomplished through a layer-by-layer electrostatic adsorption process followed by an amide bond forming reaction that had previously been employed to incorporate antibodies on screen-printed carbon[18,19] and pyrolytic graphite electrodes[50]. Glutathione (GSH)-capped AuNPs were electrostatically adsorbed onto the pencil graphite electrode using the cationic polymer PDDA, and carboxylate groups of GSH-AuNPs were activated with EDC/NHS so that amide bonds could be formed with primary amines of S100B antibodies. The presence of AuNPs on the electrode surface was confirmed using CV (Figure 13) where AuNPs get oxidized and reduced by the following half-reaction.

$$3H_2O + 2Au^o \rightleftharpoons Au_2O_3 + 6H^+ + 6e^- \tag{2}$$

AuNP-modified electrodes exhibited an oxidation peak at 1.145 V vs. Ag/AgCl, and a reduction peak at 0.653 V vs. Ag/AgCl in 0.5 M H_2SO_4, which confirms successful modification of the electrode surface with AuNPs.[18,19] Bare and PDDA-modified electrodes produced no CV peaks.
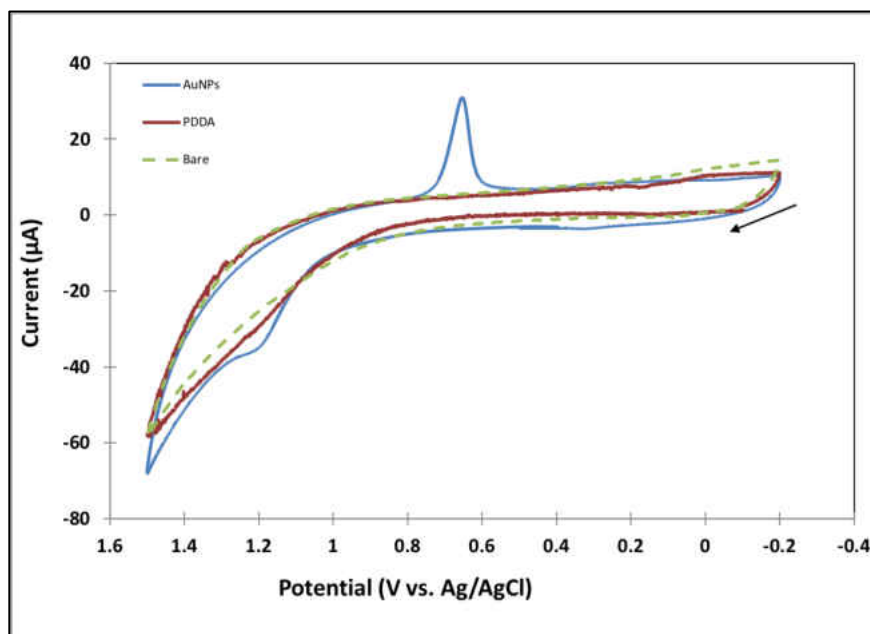
Figure 13: CVs of bare and AuNP-modified carbon electrodes in 0.5 M H_2SO_4 prepared in ultrapure water. Scan rate is 100 mV s^{-1}. Arrow indicates the direction and beginning of scan

Characterization of HRP Loading on MB Bioconjugate Using ABTS Assay

Two distinct MB bioconjugates with different ratios of HRP (11.8 µg HRP/mg MB and 1.3 µg HRP/mg MB) enzyme label to S100B detection antibody (Ab_2) were prepared by varying the amount of Ab_2 (5 µL and 20 µL, respectively) while using the same amount of HRP (5 µL) during the functionalization step. An ABTS assay was performed to determine the amount of active HRP per magnetic bead (Figure 14). Absorbance at 420 nm corresponding to product formation was linear over the range of 0 to 100 ng/mL of HRP. The amount of HRP enzyme per bead was found to be 11.8 µg HRP/mg MB for the sample with 5 µL Ab_2, while the sample with 20 µL Ab_2 contained an amount of HRP enzyme per bead that was ~9 times lower at 1.3 µg HRP/mg MB. This difference is likely the result of the competition between biotin-HRP and biotin-Ab_2 for binding sites on the streptavidin-coated MBs during the functionalization step. Higher Ab_2-to-HRP ratio during the functionalization step results in decreased HRP loading, while lower Ab_2-to-HRP ratio results in increased HRP loading.

35
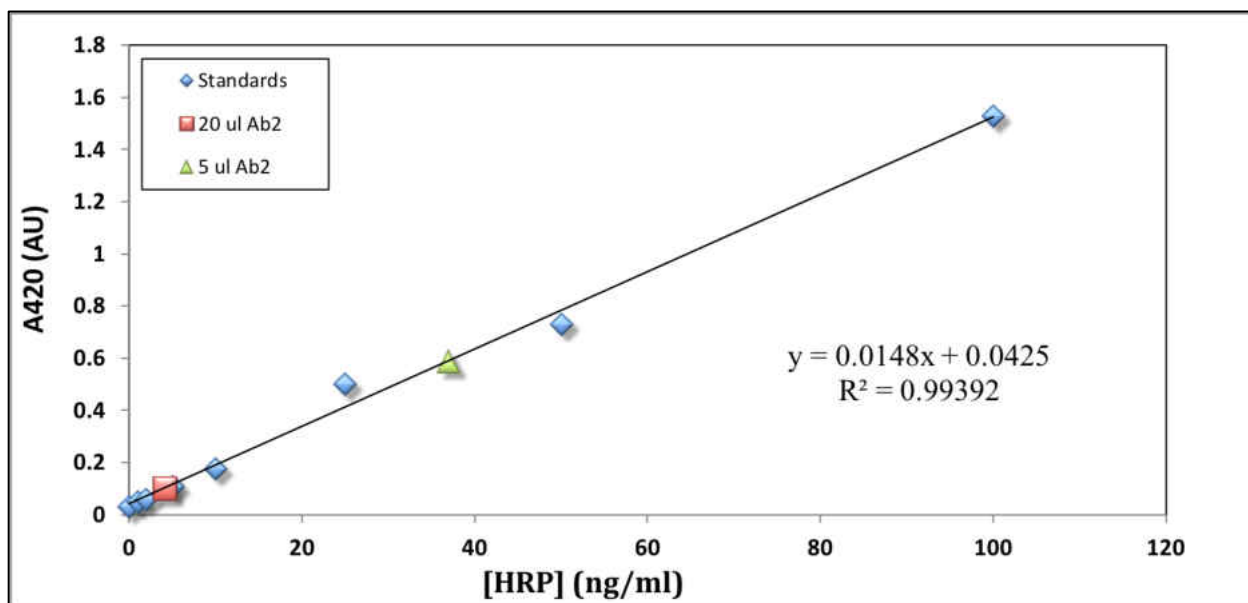
Figure 14: Characterization of HRP enzyme loading on magnetic beads using ABTS assay

Electrochemical Sandwich-Type Immunoassay in 3D-Printed Fluidic Device

For immunoassays, S100B was isolated from standards and labeled using Ab_2-MB-HRP.

$S100B$-Ab_2-MB-HRP was introduced to the electrode through the flow-injection system.

Hydrogen peroxide was then injected to activate (oxidize) HRP enzyme on the magnetic beads.

Activated HRP oxidizes hydroquinone to benzoquinone, so flow-through amperometric signal

proportional to the amount of S100B present on the electrode surface was generated by holding

the electrode at a potential where benzoquinone is reduced back to hydroquinone. To determine

an appropriate electrode potential for signal generation, CVs were performed on a solution of

hydroquinone prepared in 0.1M PBS (Figure 15). CVs of hydroquinone showed a pair of peaks

centered at 35 mV vs, Ag/AgCl with a peak separation of 112 mV and indicated that

benzoquinone is completely reduced to hydroquinone at potentials that are more negative than

~0 V vs. Ag/AgCl. To ensure complete reduction of enzyme-generated benzoquinone while

avoiding the onset of current associated with other possible reactions, a potential of -0.25 V vs.

Ag/AgCl was selected for flow-through amperometry detection during the immunoassay.
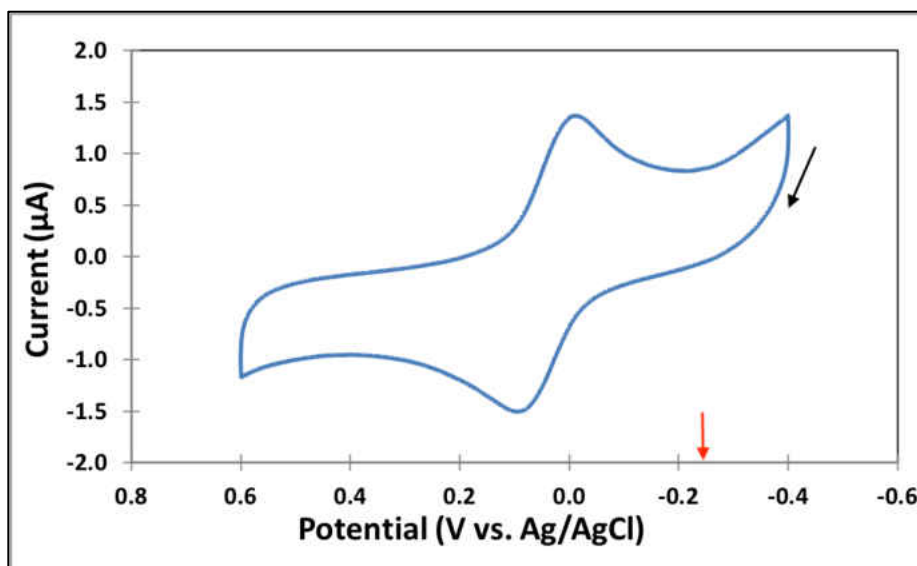
Figure 15: CV of 1.0 mM hydroquinone solution prepared in 0.1M PBS taken at 50 mV/s using electrode fitting in 3D-printed fluidic device. Scan rate is 100 mV s^{-1}, and the black arrow indicated the beginning of the scan. The red arrow indicates the potential (- 0.25 V vs. Ag/AgCl) that was selected for subsequent amperometric experiments to reduce benzoquinone generated by the activated HRP

The basis for the immunoassay is the electrochemical reduction of benzoquinone that is

generated by activated enzyme labels. Since hydrogen peroxide, which is used to activate the

enzyme during the immunoassay, is an oxidizing agent, a false positive signal would result if

H_2O_2 is able to oxidize hydroquinone to benzoquinone directly or electrocatalytically with the

aid of AuNPs immobilized on the electrode surface.[51] To confirm that S100B-Ab$_2$-MB-HRP are

necessary for generation of benzoquinone from hydroquinone, flow-through amperometry was

performed using MBs bioconjugates that were mixed with 1.45 ng/mL S100B and a separate trial

that included no MB bioconjugate (only purified water) (Figure 16). Peak-shaped amperometric

signal only resulted when MB bioconjugate was present on the surface, which confirms that the

combination of H_2O_2 and AuNPs alone cannot oxidize hydroquinone to benzoquinone.
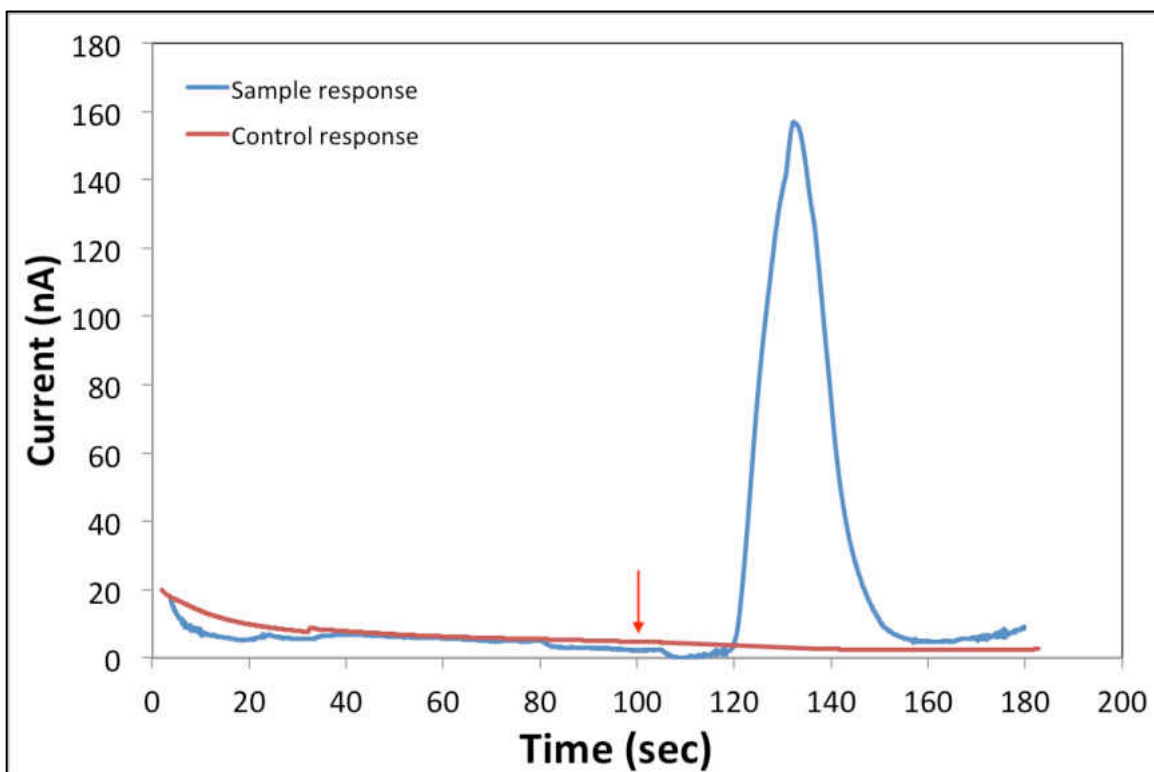
Figure 16: Comparison of amperometric results obtained in the presence and absence of MB bioconjugates. For Control, electrode was exposed to d.i. water without S100B and bioconjugate MBs. For Sample, electrode was exposed to bioconjugate MBs that were previously mixed with 1.45 ng/mL S100B. 1 mM hydroquinone with 0.1 mM H_2O_2 was injected at 100 µL/min to develop each signal. Arrow indicates that the sample was injected at 100 sec. Potential applied to working electrode was -0.25 V vs. Ag/AgCl

The Effect of HRP Loading on Amperometric Signal

Since signal generation is dependent on the amount of HRP present on the electrode surface due to binding of MBs, large amounts of HRP enzyme labels are desirable for this immunoassay. However, there is a limited number of binding sites on the MB surface, and it is necessary to also include a large number of Ab_2 on the MBs in order to facilitate binding to reach low detection limits.[52] Therefore, determining suitable HRP loading parameters is crucial to optimizing the immunoassay. To test the effects of HRP loading on flow-through amperometric signal, immunoassays were carried out with two sets of MB bioconjugates. HRP loading on MBs

38

for these two different bioconjugates were 11.8 μg HRP/mg MBs and 1.3 μg HRP/mg MBs as determined by the ABTS assay (Figure 15). MBs were mixed with either deionized water (control) or a 1.45 pg/mL S100B standard solution.

MBs with higher HRP loading produced larger signal for both control and sample (Figure 17). Notice that the amperometric signal exhibited by controls is non-zero even though the controls contain no S100B. This non-zero response can be attributed to non-specific binding of the MB bioconjugates on the electrode surface, even though steps were taken to minimize NSB. The amperometric signal using the bioconjugate MBs with higher loading of HRP (11.8 μg HRP/mg MB) was found to be 49.3 nA, which was ~1.47 times higher than the control response. The amperometric signal using the bioconjugate MBs with lower loading of HRP (1.3 μg HRP/mg MBs) was 33.7 nA, which was ~1.74 times higher than the control response. More studies must be completed to optimize HRP and antibody loading since a large analyte response and low NSB (represented by a low control response) are necessary to produce a sensitive immunoassay. However, these results suggest that this strategy can be successful as a concentration which is ~30 times lower than the detection limit reported for a commercial S100B immunoassay[55] produced a signal that is distinguishable from the control.
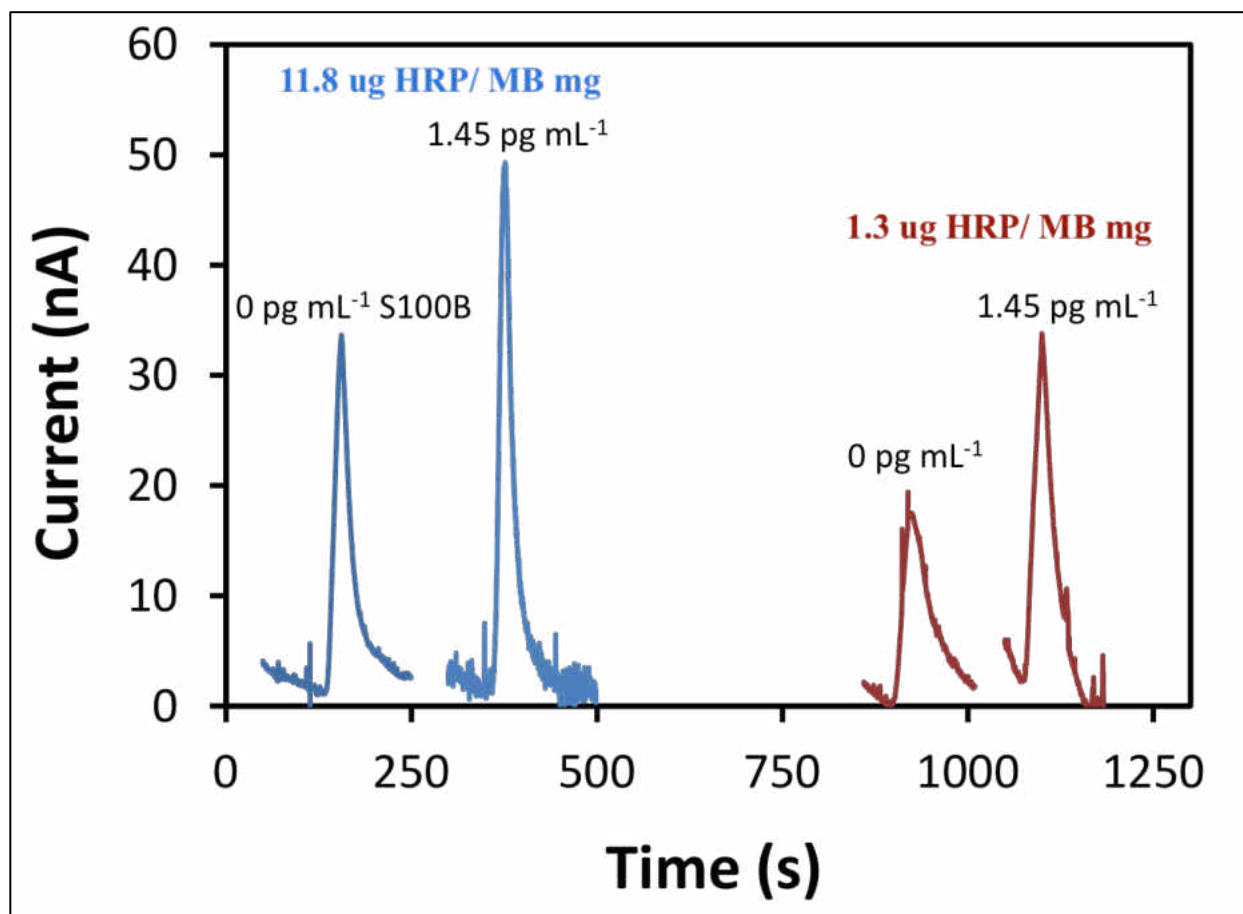
Figure 17: Effect of HRP loading on amperometric response. Curves show responses obtained using bioconjugate labels that featured 1.3 µg HRP/mg MB (red) and 11.8 µg HRP/mg MB (blue). Signal was developed by injecting 1 mM hydroquinone with 0.1 mM H_2O_2 at 100 µL/min while the working electrode was held at a potential of -0.25 V vs. Ag/AgCl

CHAPTER 4

CONCLUSION AND FUTURE WORK

Enzyme-linked immunosorbent assays (ELISA) and other clinical techniques currently used for measuring biomarker proteins are often lacking in sensitivity, affordability, speed of analysis, and capability to detect multiple biomarkers in a single sample. These limitations have sparked extensive research efforts aimed at developing simple, low-cost biosensors that are necessary to expand the possibilities of diagnostics, especially in areas of limited resources and for immediate, on-demand measurements.

3D printing has recently gained considerable interest as an adaptable and inexpensive technology for production of research tools owing to its ease of operation, speed, and capability to fabricate complex structures. The combination of 3D printed fluidics with electrochemical detection strategies seems particularly well-suited to develop biosensors that address some of the shortcomings of other measurement systems. In this project, we have demonstrated low-cost 3D-printed fluidic devices with modularly integrated electrodes can be used for electrochemical sandwich-type immunoassays for the detection of biomarker protein S100B, which is a candidate biomarker for skin cancer and brain injuries.

A B9Creator v1.2 3D printer based on a digital light processing (DLP) projector was used to fabricate robust and low-cost fluidic devices from yellow or transparent photocurable resin with 500-800 µm square cross-sectional channels. These devices cost about ~$1 in material to produce using photopolymer B9R-4-Yellow resin, and ~$0.50 using the Photopolymer PR48-clear resin. Highly conductive, low cost, and reusable electrodes were fabricated from commercially available threaded fitting and pencil rods. Fabricated electrodes cost about ~$2 all material to produce.

Electrochemical characterization experiments using the common redox probe potassium ferricyanide confirmed the functionality of the low-cost electrodes and reliability of electrochemical measurements obtained using the electrode fittings incorporated in the 3D-printed fluidic devices. Electrochemical sandwich-type immunoassays were carried out using this system for the biomarker protein S100B with HRP-MB-Ab_2 bioconjugates serving as the signal-transducing labels and detection based on flow-through amperometry.

Loading of HRP on the MB bioconjugates could be altered by adjusting the amount of HRP used during MB bioconjugate preparation. The ABTS assay was used to measure HRP loading on MB bioconjugates. Peak-shaped amperometric response only developed when HRP-MB-Ab_2 was present on the electrode surface, and the magnitudes of amperometric peaks were related to S100B concentration as well as HRP loading. Further studies must be completed to optimize HRP loading and assay conditions to reduce non-specific binding and determine important assay characteristics like sensitivity, selectivity, and dynamic range before detection of S100B in real patient samples can be attempted. Upon repolishing, a set of 14 electrodes gave stable, reproducible conductivity for more than four months even after they were used for several experiments.

While these studies were focused on demonstrating feasibility of electrochemical immunoassays using flow-through amperometric detection in 3D-printed fluidic devices for a single biomarker protein, simultaneous detection of multiple biomarker proteins (multiplexed detection) is also possible using this system. To enable multiplexed biomarker detection in this system, electrode fittings with two graphite working electrodes have been fabricated (Figure 18) in a similar fashion to that previously demonstrated.[21,22,23]
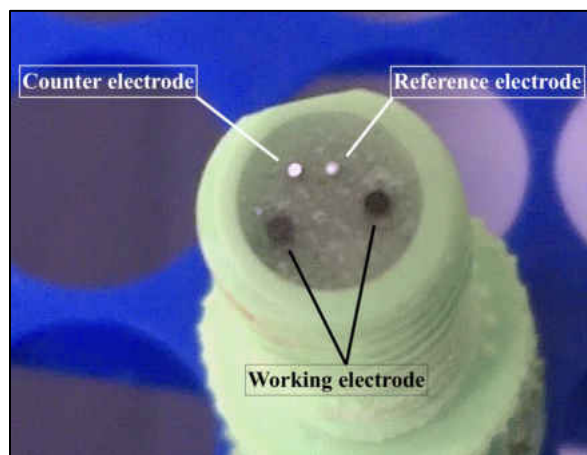
Figure 18: Photograph of two-working electrode system. Working electrodes were fabricated from 5-10 mm long carbon (pencil graphite) rods (0.5 mm in diameter), reference electrode was fabricated from silver wire (0.25 mm in diameter), and counter electrode was fabricated from 22-gauge stainless steel (SS) wire (0.64 mm in diameter)

The electrochemical behaviors of the two working electrodes towards common redox probe $K_3[Fe(CN)_6]$ were in agreement (Figure 19). Future efforts will be focused on further refining multielectrode platforms for this system and conducting immunoassay measurements of biomarker panels, where issues like cross-reactivity and electrode spacing must also be considered.
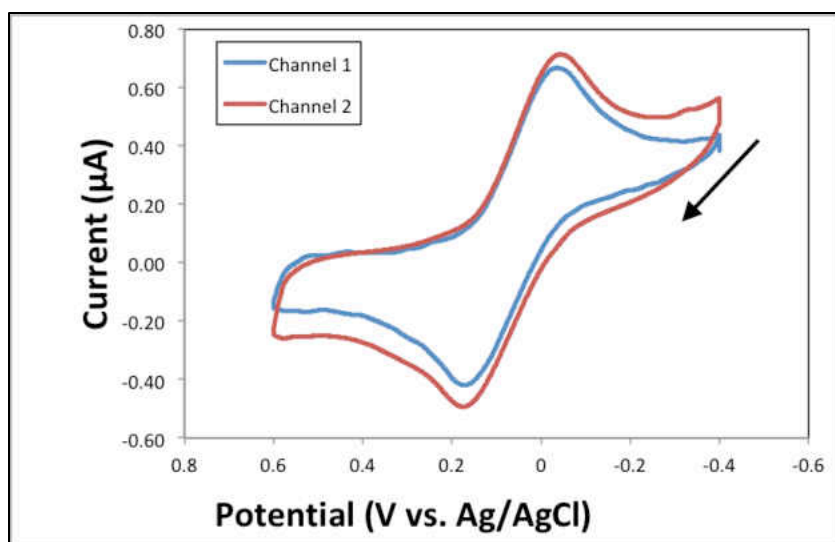

Figure 19: CV responses of electrode fitting with two pencil graphite working electrodes. The two working electrodes positioned in the same fitting were immersed in a solution that contained $K_3[Fe(CN)_6]$ with 0.1 M KCl prepared in ultrapure water. Scan rate was 100 mV/s. Arrow indicates the direction and beginning of scan

REFERENCES

(1) Mayeux, R. Biomarkers: Potential Uses and Limitations. *NeuroRX* **2004**, 1, 182–188.

(2) Strimbu, K.; Tavel, J. A. What Are Biomarkers? *Curr. Opin. HIV. AIDS* **2010**, 5, 463–466.

(3) Kumar, A.; Gangadharan, B.; Cobbold, J.; Thursz, M.; Zitzmann, N. Absolute quantitation of disease protein biomarkers in a single LC-MS acquisition using apolipoprotein F as an example. *Sci. Rep.* **2017**, 7, 12072.

(4) Wu, J.; Fu, Z.; Yan, F.; Ju, H. Biomedical and clinical applications of immunoassays and immunosensors for tumor markers. *Trac-Trend. Anal. Chem.* **2007**, 26, 679-688.

(5) Vashist, S. K.; Luppa, P. B.; Yeo, L. Y.; Ozcan, A.; Luong, J. H. T. Biomedical and clinical applications of immunoassays and immunosensors for tumor markers. *Trends. Biotechnol.* **2015**, 33, 692–705.

(6) Rusling, J. F. Multiplexed Electrochemical Protein Detection and Translation to Personalized Cancer Diagnostics. *Anal. Chem.* **2013**, 85, 5304–5310.

(7) Lee, H. J.; Wark, A. W.; Corn, R. M. Microarray methods for protein biomarker detection. *Analyst* **2008**, 133, 975− 983.

(8) Rusling, J. F. Electrochem. Soc. Cancer Diagnostics Using ECL Detection. *Electrochem. Soc. Interface.* **2016**, 25, 47–51.

(9) Rusling, J. F.; Kumar, C. V.; Gutkind, J. S.; Patel, V. Measurement of biomarker proteins for point-of-care early detection and monitoring of cancer. *Analyst* **2010**, 135, 2496–2511.

(10) Xu, S.; Liu, Y.; Wang, T.; Li, J. Positive Potential Operation of a Cathodic Electrogenerated Chemiluminescence Immunosensor Based on Luminol and Graphene for Cancer Biomarker Detection. *Anal. Chem.* **2011**, 83, 3817–3823.

(11) Burcu Bahadır, E.; Kemal Sezgintürk, M. Applications of electrochemical immunosensors for early clinical diagnostics. *Talanta* **2015**, 132, 162–174.

(12) Ronkainen, N. J.; Halsall, H. B.; Heineman, W. R. Electrochemical biosensors. *Chem. Soc. Rev.* **2010**, 39, 1747–1763.

(13) W. R. Heineman and H. B. Halsall. Strategies for Electrochemical Immunoassay. *Anal. Chem.* **1985**, 75, 1321A–1331A.

(14) Choi, J.; Oh, K. W.; Han, A.; Wijayawardhana, C. A.; Lannes, C.; Bhansali, S.; Schlueter, K. T.; Heineman, W. R.; Halsall, H. B.; Nevin, J. H.; et al. Development and Characterization of Micro̅uidic Devices and Systems for Magnetic Bead-Based Biochemical Detection. *Biomed. Microdevices.* **2001**, 3, 191.

(15) Bange, A.; Halsall, H. B.; Heineman, W. R. Microfluidic immunosensor systems. *Biosens. Bioelectron.* **2005**, 20, 2488–2503.

(16) Chikkaveeraiah, Liu, Mani, Papadimitrakopoulos, & Rusling. A microfluidic electrochemical device for high sensitivity biosensing: Detection of nanomolar hydrogen peroxide. *Electrochem. Commun.* **2009**, 11, 819-822.

(17) Qiang, Vaddiraju, Rusling, & Papadimitrakopoulos. Highly sensitive and reusable Pt-black microfluidic electrodes for long-term electrochemical sensing. *Biosens. Bioelectron.* **2010**, 26, 682-688.

(18) Chikkaveeraiah, B. V.; Mani, V.; Patel, V.; Gutkind, J. S.; Rusling, J. F. Microfluidic electrochemical immunoarray for ultrasensitive detection of two cancer biomarker proteins in serum. *Biosens. Bioelectron.* **2011**, 26, 4477–4483.

(19) Malhotra, R.; Patel, V.; Chikkaveeraiah, B. V.; Munge, B. S.; Cheong, S. C.; Zain, R. B.; Abraham, M. T.; Dey, D. K.; Gutkind.; J. S.; Rusling, J. F. Ultrasensitive Detection of Cancer Biomarkers in the Clinic by Use of a Nanostructured Microfluidic Array. *Anal. Chem.* **2012**, 84, 6249–6255.

(20) Chan, H. N.; Tan, M. J. A.; Wu, H. Point-of-Care Testing: Applications of 3D Printing. *Lab. Chip.* **2017**, *17*, 2713–2739.

(21) Bishop, G. W.; Satterwhite, J. E.; Bhakta, S.; Kadimisetty, K.; Gillette, K. M.; Chen, E.; Rusling, J. F. 3D-Printed Fluidic Devices for Nanoparticle Preparation and Flow-Injection Amperometry Using Integrated Prussian Blue Nanoparticle- Modified Electrodes. *Anal. Chem.* **2015**, 87, 5437–5443.

(22) J. L. Erkal, A. Selimovic, B. C. Gross, S. Y. Lockwood, E. L. Walton, S. McNamara, R. S. Martin, D. M. Spence. 3D Printed Microfluidic Devices with Integrated Versatile and Reusable Electrodes. *Lab. Chip.* **2014**, 14, 2023-2032.

(23) Bishop, G. W.; Satterwhite-Warden, J. E.; Bist, I.; Chen, E.; Rusling, J. F. Electrochemiluminescence at Bare and DNA-Coated Graphite Electrodes in 3D-Printed Fluidic Devices. *ACS. Sens.* **2016**, 1, 197–202.

(24) Chan, H. N.; Shu, Y.; Xiong, B.; Chen, Y.; Chen, Y.; Tian, Q.; Michael, S. A.; Shen, B.; Wu, H. Simple, Cost-Effective 3D Printed Microfluidic Components for Disposable, Point-of-Care Colorimetric Analysis. *ACS. Sens.* **2016**, 1, 227–234.

(25) Rengier, F.; Mehndiratta, A.; Tengg-Kobligk, H. von; Zechmann, C. M.; Unterhinninghofen, R.; Kauczor, H.-U.; Giesel, F. L. 3D printing based on imaging data: review of medical applications. *Int. J. CARS.* **2010**, 5, 335–341.

(26) Ambrosi, A.; Pumera, M. 3D-printing technologies for electrochemical applications. *Chem. Soc. Rev.* **2016**, 45, 2740–2755.

(27) Shallan, A. I.; Smejkal, P.; Corban, M.; Guijt, R. M.; Breadmore, M. C. Cost-Effective Three-Dimensional Printing of Visibly Transparent Microchips within Minutes. *Anal. Chem.* **2014**, 86, 3124–3130.

(28) Gross, B. C.; Erkal, J. L.; Lockwood, S. Y.; Chen, C.; Spence, D. M. Evaluation of 3D printing and its potential impact on biotechnology and the chemical sciences. *Anal. Chem.* **2014**, 86, 3240–3253.

(29) Gong, H.; Bickham, B. P.; Woolley, A. T.; Nordin, G. P. Custom 3D Printer and Resin for 18 μm × 20 μm Microfluidic Flow Channels. *Lab. Chip.* **2017**, 17, 2899–2909.

(30) Ventola, C. L. Medical Applications for 3D Printing: Current and Projected Uses. *P&T.* **2014**, 39, 704–711.

(31) Gong, H.; Beauchamp, M.; Perry, S.; Woolley, A. T.; Nordin, G. P. Optical approach to resin formulation for 3D printed microfluidics. *RSC. Adv.* **2015**, 5, 106621–106632.

(32) Waheed, S.; Cabot, J. M.; Macdonald, N. P.; Lewis, T.; Guijt, R. M.; Paull, B.; Breadmore, M. C. 3D printed microfluidic devices: enablers and barriers. *Lab. Chip.* **2016**, 16, 1993 2013.

(33) Beauchamp, M. J.; Nordin, G. P.; Woolley, A. T. Moving from millifluidic to truly microfluidic sub-100-μm cross-section 3D printed devices. *Anal. Bioanal. Chem.* **2017**, 409, 4311–4319.

(34) Snowden, M. E.; King, P. H.; Covington, J. A.; Macpherson, J. V.; Unwin, P. R. Fabrication of Versatile Channel Flow Cells for Quantitative Electroanalysis Using Prototyping. *Anal. Chem.* **2010**, 82, 3124–3131.

(35) Rogers, C. I.; Qaderi, K.; Woolley, A. T.; Nordin, G. P. 3D printed microfluidic devices with integrated valves. *Biomicrofluidics* **2015**, 9, 1-9.

(36) American Cancer Society. Cancer Facts & Figures 2017. Atlanta, GA: American Cancer Society, 2017.

(37) H. K. Weir, T. D. Thompson, A. Soman, B. Møller, S. Leadbetter. The Past, Present, and Future of Cancer Incidence in the United States: 1975-2020. *Cancer* **2015**, 121, 1827-1837.

(38) S. T. Chen, A. C. Geller, H. Tsao. Update on the Epidemiology of Melanoma. *Curr. Derm. Rep.* **2013**, 2, 25-34.

(39) Z. Apalla, D. Nashan, R. B. Weller, X. Castellsagué. Skin Cancer: Epidemiology, Disease Burden, Pathophysiology, Diagnosis, and Therpeutic Approaches. *Dermatol. Ther.* **2017**, 7, S5-S19.

(40) H. M. Kluger, K. Hoyt, A. Bacchiocchi, T. Mayer, J. Kirsch, Y. Kluger, M. Sznol, S. Ariyan, A. Molinaro, R. Halaban. Plasma Markers for Identifying Patients with Metastatic Melanoma. *Clin. Cancer.Res.* **2011**, 17, 2417-2425.

(41) D. Weinstein, J. Leininger, C. Hamby, B. Safai. Diagnostic and Prognostic Biomarkers in Melanoma. *J. Clin. Aesthet. Dermatol.* **2014**, 7, 13-24.

(42) E. D. Mårtenson, L. O. Hansson, B. Nilsson, E. von Schoultz, E. M. Brahme, U. Ringborg, J. Hansson. Serum S- 100B Protein as a Prognostic Marker in Malignant Cutaneous Melanoma. *J. Clin. Oncol*. **2001**, 19, 824-831.

(43) Harpio, R.; Einarsson, R. S100 Proteins as Cancer Biomarkers with Focus on S100B in Malignant Melanoma. *Clin. Biochem*. **2004**, 37 (7), 512–518.

(44) Zheng, M.; Huang, X. J. Nanoparticles Comprising a Mixed Monolayer for Specific Bindings with Biomolecules. *Am. Chem. Soc.* **2004**, 126, 12047–12054.

(45) Rusling, J. F.; Bishop, G. W.; Doan, N. M.; J. Mater. Nanomaterials and biomaterials in electrochemical arrays for protein detection. *Chem. B.* **2013**, 2, 12–30.

(46) Krause, C. E.; Otieno, B. A.; Bishop, G. W.; Phadke, G.; Choquette, L.; Lalla, R. V.; Peterson, D. E.; Rusling, J. F. Ultrasensitive microfluidic array for serum pro-inflammatory cytokines and C-reactive protein to assess oral mucositis risk in cancer patients. *Anal Bioanal. Chem* **2015**, 407, 7239–7243.

(47) Rogers, C. I.; Pagaduan, J. V.; Nordin, G. P.; Woolley, A. T. Single-monomer formulation of polymerized polyethylene glycol diacrylate as a nonadsorptive material for microfluidics. *Anal Chem.* **2011**, 83, 6418–6425.

(48) Au, A. K.; Bhattacharjee, N.; Horowitz, L. F.; Chang, T. C.; Folch, A. 3D-Printed Microfluidic Automation. *Lab. Chip.* **2015**, 15, 1934–1941.

(49) Takenaga, S.; Schneider, B.; Erbay, E.; Biselli, M.; Schnitzler, T.; Schöning, M. J.; Wagner, T. 3D-Printed Microfluidic Automation. *Phys. Status. Solidi. A.* **2015**, 212, 1347–1352.

(50) Mani, V.; Chikkaveeraiah, B. V.; Patel, V.; Gutkind, J. S.; Rusling, J. F. Ultrasensitive Immunosensor for Cancer Biomarker Proteins Using Gold Nanoparticle Film Electrodes and Multienzyme-Particle Amplification. *ACS. Nano.* **2009**, *3* (3), 585–594.

(51) Etesami, M.; Salehi, F.; Mohamed, N. Electrooxidation of Hydroquinone on Simply Prepared Au-Pt Bimetallic Nanoparticles. *Sci. China. Chem.* **2013**, 56, 746–754.

(52) Mani, V.; Wasalathanthri, D. P.; Joshi, A. A.; Kumar, C. V.; Rusling, J. F. Highly Efficient Binding of Paramagnetic Beads Bioconjugated with 100,000 or More Antibodies to Protein-Coated Surfaces. *Anal. Chem.* **2012**, 84, 10485–10491.

(53) TechNotes | Bangs Laboratories, Inc. https://www.bangslabs.com/support/technical-support/technotes (accessed Jun 12, 2018).

(54) ABTS Substrate Tablets - Thermo Fisher Scientific https://www.thermofisher.com/order/catalog/product/34026 (accessed Jun 12, 2018).

(55) Human S100B DuoSet ELISA DY1820-05: R&D Systems https://www.rndsystems.com/products/human-s100b-duoset-elisa_dy1820-05 (accessed Jun 12, 2018).

VITA

ABDULHAMEED ALABDULWAHEED

Education:	B.S. Chemistry, College of Science, King Faisal University, Al Ahssa, Kingdom of Saudi Arabia, 2010. M.S. Chemistry, East Tennessee State University, Johnson city, Tennessee, 2018.
Professional Experience:	Research assistant, College of Science, King Faisal University; Al Ahssa, Kingdom of Saudi Arabia, 2010-2011. Teacher assistant, College of Science, King Faisal University; Al Ahssa, Kingdom of Saudi Arabia, 2012-2014. Participating with poster presentation at the Southeastern Regional Meeting of the American Chemical Society (SERMACS), 2017 Participating with poster presentation at the Appalachian Student Research Forum arranged by East Tennessee University, 2017 and 2018.
Honors and Awards:	First place award in the Masters Natural Sciences for poster presentation at the Appalachian Student Research Forum arranged by East Tennessee University, 2018.